Life Sciences in Space Research 1 (2014) 2–9

Contents lists available at ScienceDirect

Life Sciences in Space Research

www.elsevier.com/locate/lssr

Review article

Space radiation protection: Destination Mars

Marco Durante [a,b,*]

[a] GSI Helmholtz Center for Heavy Ion Research, Biophysics Department, Darmstadt, Germany
[b] Technical University of Darmstadt, Institute of Condensed Matter Physics, Darmstadt, Germany

ARTICLE INFO

Article history:
Received 6 January 2014
Received in revised form 18 January 2014
Accepted 20 January 2014

Keywords:
Space radiation
Mars mission
Shielding
Magnetic shielding
Nuclear electric rockets

ABSTRACT

National space agencies are planning a human mission to Mars in the XXI century. Space radiation is generally acknowledged as a potential showstopper for this mission for two reasons: a) high uncertainty on the risk of radiation-induced morbidity, and b) lack of simple countermeasures to reduce the exposure. The need for radiation exposure mitigation tools in a mission to Mars is supported by the recent measurements of the radiation field on the Mars Science Laboratory. Shielding is the simplest physical countermeasure, but the current materials provide poor reduction of the dose deposited by high-energy cosmic rays. Accelerator-based tests of new materials can be used to assess additional protection in the spacecraft. Active shielding is very promising, but as yet not applicable in practical cases. Several studies are developing technologies based on superconducting magnetic fields in space. Reducing the transit time to Mars is arguably the best solution but novel nuclear thermal-electric propulsion systems also seem to be far from practical realization. It is likely that the first mission to Mars will employ a combination of these options to reduce radiation exposure.

1. Introduction

The risks of the space travel have been comprehensively summarized in the NASA Bioastronautics Roadmap, now updated in the Human Research Roadmap (NASA, 2005), and current gaps in knowledge also identified. Risks were rated from 1 (risk of serious health effects, and mission could be impossible without mitigation) to 3 (suspected health consequences with limited impact on the mission design). The risks can be summarized into three broad categories:

1. Physiological problems caused by microgravity (or reduced gravity)
2. Psychological and medical problems caused by isolation
3. Acute and late risks caused by exposure to radiation

The physiological changes due to weightlessness have been extensively studied, especially during long-term missions on space stations (International Space Station, ISS, and, previously, Mir) in low-Earth-orbit (LEO). Bone loss, kidney stone formation, skeletal muscle mass reduction, cardiovascular alterations, impaired sensory-motor capabilities, immune system dysfunctions are among the consequences of prolonged stays in microgravity. The risks are very well characterized, and several countermeasures are available. None of these risks are rated 1 in the Bioastronautics roadmap.

Isolation may lead to serious neurobehavioral problems caused by poor psychosocial adaptation. Several ground platforms are used to study these problems and develop countermeasures, such as the Concordia base in Antarctica and the Mars500 isolation experiments currently under way in Russia. Isolation also brings the problem of autonomous medical care (AMC), i.e. the capability to handle sickness or accidents in complete isolation. This is clearly a risk category 1 for the mission to Mars. Countermeasures for AMC risks are mostly technological, i.e. rely on the development of portable medical equipment and telemedicine.

Finally, there are the risks related to exposure to space radiation. Because of the complex nature of the space radiation environment (Durante and Cucinotta, 2011), both acute (i.e. short-term risk of radiation sickness) and late (e.g. cancer) effects are possible. Acute radiation syndrome (ARS) can be caused by intense solar particle events (SPE) with crews unable to reach adequate shielding. Late radiation morbidity is associated with the chronic exposure to galactic cosmic radiation (GCR), which is substantially different both qualitatively and quantitatively from the Earth's radiation natural background. Because of the qualitative difference in the radiation spectrum (γ-, β- and α-rays on Earth; protons and heavy ions in space), terrestrial data cannot be extrapolated to space radiation exposure scenarios. Therefore, the uncertainty in radiation risk estimates is very high, especially for

* Correspondence to: GSI Helmholtzzentrum für Schwerionenforschung, Biophysik Abteilung, Planckstraße 1, 64291 Darmstadt, Germany. Tel.: +49 (0)6159 71 2009.
E-mail address: M.Durante@gsi.de.

http://dx.doi.org/10.1016/j.lssr.2014.01.002
2214-5524/

Table 1
GCR dose in different mission scenarios based on the recent MSL measurements (Zeitlin et al., 2013; Hassler et al., 2014). Inspiration Mars is a 501 flyby mission. Mars sortie assumes a 30-days stay on the planet, and Mars base 500 days. Both those design reference missions (Tito et al., 2013) assume a 180 cruise to/from Mars.

	GCR dose rate (mGy/day)	GCR dose-equivalent rate (mSv/day)	Inspiration Mars (Sv)	Mars sortie (Sv)	Mars base (Sv)
MSL cruise (Zeitlin et al., 2013)	0.46	1.84	0.92	0.7	0.98
MSL on Mars (Hassler et al., 2014)	0.21	0.64			

carcinogenesis, central nervous system (CNS) damage, and late cardiovascular damage. Early estimates of the uncertainty on space radiation cancer mortality risk ranged from 400% to 1500%, with more precise estimates showing uncertainties at the 95% confidence level of 4-fold times the point projection (Durante and Cucinotta, 2008). Moreover, countermeasures are not readily available. A fundamental tenet of radiation protection is that there are three means to reduce exposure to ionizing radiation: increasing the distance from the radiation source, reducing the exposure time, and by shielding. Distance is not an issue in space, GCR being isotropic. Time in space should be increased rather than decreased according to the plans of exploration and colonization, although reduction of the transit time to the planet, where heavy shielding can be more easily achieved, may contribute to reducing radiation exposure (Durante and Bruno, 2010).

2. The Mars mission

The manned mission to Mars is considered the main goal of human exploration by all national space agencies, whose combined efforts are discussed in the International Space Exploration Coordination Group (ISECG) (ISECG, 2013). The ISECG roadmap considers a stepwise approach to Mars colonization, including asteroids and lunar missions.

NASA's "Design Reference" Mars mission (Drake et al., 2010) analyzes different scenarios, with a typical figure of about 180 days for the cruise duration (each way) and 30 (Mars sortie) to 500 (Mars base) days on the planet. In April 2013, Dennis Tito proposed Inspiration Mars, a manned mission planned for 2018. One male and one female astronaut will travel in a free-return (flyby) 501-days interplanetary flight starting in January 2018 (or 2031) to exploit the favorable reduced distance of the Earth–Mars trajectories (Tito et al., 2013). Inspiration Mars has relatively simple mission architecture and would exploit rockets with conventional technologies, such as the recently developed Falcon Heavy (53 tons to LEO, 10 tons to Mars) by SpaceX.

The measurements of the Radiation Assessment Detector (RAD) instrument on the Mars Science Laboratory (MSL) during the cruise to Mars (Zeitlin et al., 2013) and on the planet's surface (Hassler et al., 2014) can be used to estimate the dose in different Mars mission scenarios (Table 1). Measurements were accumulated around the 2012–2013 solar maximum activity. Even though the mission was around the solar maximum period, SPE only contributed 5% to the total dose during the journey (Zeitlin et al., 2013), perhaps because the present solar maximum is relatively weak. During solar minimum the solar magnetic field is reduced and the GCR equivalent dose rate can be up to two times higher (Durante and Cucinotta, 2011). However, the actual dose rate within the spacecraft will depend on the shielding. Therefore, in our exercise, we used the MSL measurement in all mission scenarios. It is interesting to see that most of the dose is incurred during cruise phase (Table 1). The dose on the planet can be further reduced using bases with heavy shielding, exploiting in situ planetary materials.

Estimates of the dose in Table 1 can be converted into estimated excess relative cancer risk (ERR) coefficients. ERR for cancer death risk can be derived from the latest Report 14 (Ozasa et al., 2012) of the Radiation Effects Research Foundation (RERF). Lifetime absolute excess cancer risk (%) is given by the product of the ERR and the background cancer death risk. Background site- and gender-specific mortality for cancer is derived from the most recent statistics in the USA population (Siegel et al., 2013). Cancer risk coefficients in the mission to Mars should be scaled compared to the A-bomb survivor data to account for radiation quality and low dose-rate exposure. Radiation quality is already included in the MSL measurement, which provided a mean quality factor of 3.82 in deep space (Zeitlin et al., 2013) and 3.05 on Mars (Hassler et al., 2014). For the dose- and dose-rate effectiveness factor (DDREF) the current uncertainty is very high (Durante and Cucinotta, 2008). According to the most recent BEIRVII report (National Research Council, 2006), in this exercise a DDREF = 1.5 is used to scale the ERR from the Report 14 (Ozasa et al., 2012) to the space environment (Table 2).

Table 2
Excess relative risk (ERR) and lifetime excess mortality risk (%) for the male and female astronauts at 30 years of age at the time of the Inspiration Mars mission.

	ERR		Background mortality in USA (%)	Excess risk (%)	
	Male	Female		Male	Female
All solid cancers	0.166	0.249	22	3.802	7.285
Noncancer diseases	0.080		71	5.592	

Cancer is not the only late risk attributable to cosmic ray exposure. Noncancer effects, e.g. CNS and cardiovascular diseases, may also impact astronauts' health, and the uncertainty on these radiation-induced effects is even higher than for cancer (Durante and Cucinotta, 2008). RERF data demonstrate an increase in noncancer death risk in A-bomb survivors, largely driven by cardiovascular and pulmonary morbidity (Ozasa et al., 2012). A comparison of radiogenic cancer and noncancer risks in the Inspiration Mars (Tito et al., 2013) scenarios is provided in Table 2. Absolute mortality for cancer and noncancer diseases refers to the general US population (Siegel et al., 2013). ERR for noncancer mortality was estimated using the linear dose model, in which city, sex, age at exposure, and attained age were included in the background rates, but not allowing radiation effect modification by those factors (Ozasa et al., 2012). These ERR are compared to those for solid cancers at 30 years of age. We used the same DDREF for cancer and noncancer diseases. Females have a higher cancer risk than males, mostly driven by the breast cancer ERR. The results in Table 2 suggest that the risk for Inspiration Mars would exceed the 3% excess cancer risk originally used by NASA for career limits of astronauts in LEO (NASA, 2005). New NASA radiation standards limit astronaut exposures to a 3% risk of exposure induced death (REID) at the upper 95% confidence interval (CI) of the risk estimate (NASA, 2007). Using the NASA model for the REID, Cucinotta et al. (2013) recently estimated the combined REID for cancer and circulatory diseases and related uncertainties for different Mars mission scenarios. The REID calculations show that the 3% limit at 95% CI would be exceeded for both Mars conjunction and opposition missions (Cucinotta et al., 2013).

The MSL measurements (Zeitlin et al., 2013; Hassler et al., 2014) and corresponding health risk estimates (Cucinotta et al., 2013) clearly point to radiation as a major health hazard for the Mars mission. Reduction of the risk uncertainty can only be achieved by extensive research programs, especially ground-based

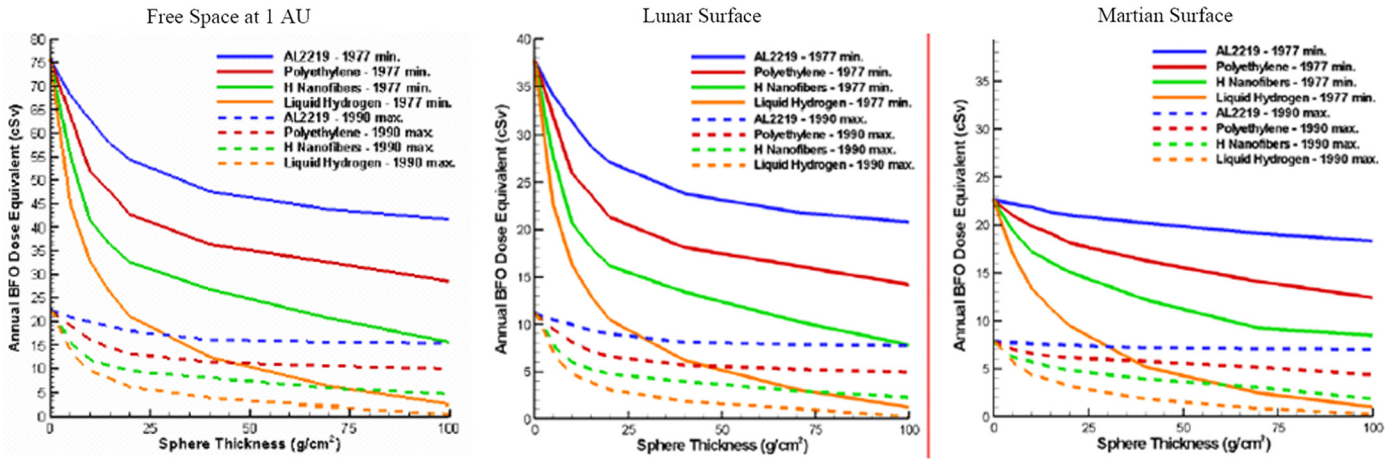

Fig. 1. Estimated impact of the shielding using different materials (aluminum, polyethylene, hydrogen nanofibers or liquid hydrogen) on the annual dose equivalent. The dose is calculated in the blood forming organs (BFO) using the radiation environment data relative to the 1977 solar minimum (solid lines) or 1990 solar maximum (dashed lines). Simulations using HZETRN are for deep space, moon or Mars surface (without albedo neutrons and pion-electromagnetic cascade). Modified from Wilson et al. (1997), courtesy of NASA.

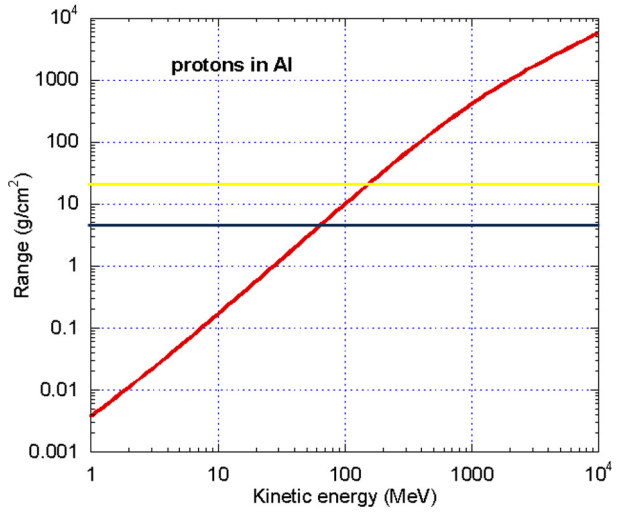

Fig. 2. Energy-range relationship for protons in aluminum. The range is expressed in g/cm^2, Al density is 2.7 g/cm^3. Horizontal lines represent typical thickness of the Al spacecraft walls (5 g/cm^2, green line) and the effective thickness due to the presence of payloads and racks (20 g/cm^2, yellow line). Ranges were calculated by SRIM2013 (http://www.srim.org/). (For interpretation of the references to color in this figure legend, the reader is referred to the web version of this article.)

radiobiology studies at particle accelerators (Durante and Kronenberg, 2005). Development of biological countermeasures is discussed in a review paper in this journal issue (Kennedy, 2014). Physical countermeasures will be discussed below.

3. Passive shielding

For terrestrial radiation workers, additional protection against radiation exposure is usually provided through increased shielding. Unfortunately, shielding in space is problematic, especially when GCR is considered. High-energy radiation is very penetrating: a thin or moderate shielding is generally efficient in reducing the equivalent dose, but as the thickness increases, shield effectiveness drops (Fig. 1) (Wilson et al., 1997). This is the result of the production of a large number of secondary particles, including neutrons, caused by nuclear interactions of the GCR with the shield. These particles have generally lower energy, but can have higher quality factors than incident cosmic primary particles.

In addition, shields obviously pose mass problems. A heavy load, added purely for reducing radiation exposures, incurs a substantial mass penalty for launch and therefore may dramatically increase mission cost. Typical shielding provided by the spacecraft wall is around 5 g/cm^2 Al, but the effective shield on ISS is close to 20 g/cm^2 Al in several locations, because of the presence of several payloads and racks. This Al thickness is able to stop all protons at energies below 100–200 MeV (Fig. 2), and is therefore efficient for trapped radiation and most SPE (Durante and Cucinotta, 2011). Protons with energies above a few MeV can penetrate the skin and deposit their energy in inner body organs. A “storm shelter”, i.e. a small area with heavy shield (>20 g/cm^2 Al), can be included in the spacecraft for protection against large SPE. Most SPE last less than two days, and the most intense portion is generally few hours. During this limited period, the crew can move in this small area for emergency protection.

As shown in Fig. 1, shielding of GCR is much more problematic than for SPE. The basic physics is relatively simple (Durante and Cucinotta, 2011), because the energy loss of heavy ions in the shield is caused by electron and nuclear interactions, which can be approximated by the well-known Bethe–Bloch and Bradt–Peters equations:

$$S = \frac{4\pi Z_P^2 \rho Z_T N_A e^4}{A_T m \beta^2 c^2}\left[\left\{\ln\left(\frac{2mc^2\beta^2\gamma^2}{I}\right) - \beta^2 - \frac{C(\beta)}{Z_T} + Z_P L_1(\beta) + Z_P^2 L_2(\beta) + L_3(\beta)\right\}\right] \quad (1)$$

$$\sigma = \pi r_0^2 c_1(E)\left(A_P^{1/3} + A_T^{1/3} - c_2(E)\right)^2 \quad (2)$$

where S is the stopping power (or linear energy transfer, LET), σ the fragmentation cross-section, e the electronic charge, N_A the Avogadro number, ρ the target density, m the mass of the electron, c the speed of light, $\beta = v/c$, I the mean excitation energy, A_p and A_T the atomic weight of the projectile and target, respectively, and r_0 the nucleon radius. In Eq. (1), the various correction terms are the shell correction $C(\beta)$, Barkas correction, $L_1(\beta)$, Bloch term, $L_2(\beta)$, and Mott and density corrections $L_1(\beta)$. In Eq. (2), energy-dependent corrections to the geometrical cross-section are provided by the semi-empirical terms c_1 and c_2. If we consider the mass stopping power and the fragmentation cross-section per unit target mass, Eqs. (1) and (2) show that:

$$\frac{S}{\rho} \propto \frac{Z_T}{A_T}; \qquad \frac{\sigma}{A_T} \propto A_T^{-\frac{1}{3}} \quad (3)$$

So that both electromagnetic and nuclear energy deposition per unit target mass decrease by increasing the atomic weight A_T of

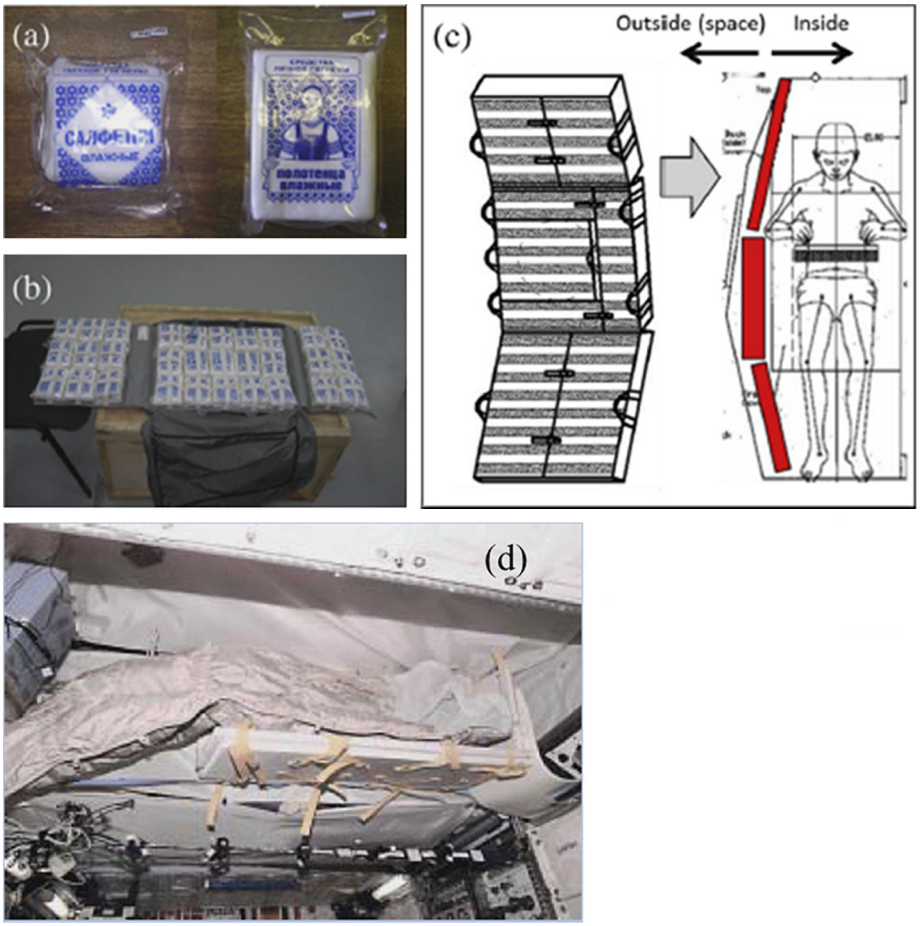

Fig. 3. Examples of shielding with low-Z materials installed on the ISS. Protective curtain on the Russian Module, (a) hygienic wipes and towels, (b) stack board, and (c) schematic drawing of stack board and its installation in the ISS Russian Module. Figures from Kodaira et al. (2014), reproduced with permission. (d) Polyethylene panels installed in the crew sleeping quarters of the ISS NASA module. Picture from NASA, Office of Biological and Physical Research.

the shield. Therefore, light materials are more effective for shielding in space (Wilson et al., 1997) and liquid hydrogen has the maximum performance as shield material (Fig. 1). Hydrogen is not a practical shield material, being a low temperature liquid. Hydrogen storage in graphite nanofibers or lithium hydride (^{6}LiH) may have a large impact in space shield design. So far, it appears that polyethylene can be a good compromise. NASA has used aluminum panels with lighter polyethylene slabs in the crew sleeping quarters on ISS (Fig. 3). Dose measurements were consistent with the expected dose reduction of around 20% in the shielded area (Shavers et al., 2004).

Water is also a light shielding, and is abundant on ISS and any spacecraft with a life-support system. A "protective curtain" can be built using stacks of humid hygienic wipes and towels (Fig. 3). A protective curtain of 6.3 g/cm^2 (total mass 67 kg) was installed along the outer wall of the starboard crew cabin in the Russian Service Module of the ISS (Kodaira et al., 2014). A dose equivalent reduction around 37% was measured on the ISS in 2010 using passive dosimeters. The protective curtain can be an effective and simple shielding not only for trapped radiation, but also for low-energy GCR.

Data in Fig. 1 are calculated using an earlier version of the HZETRN code developed by NASA (Wilson et al., 1991), which considered only a reduced isotopic grid of 59 particles. Recent extensions of the code have added multigroup methods for bidirectional neutron transport and pion transport coupled to the GCR sources (Slaba et al., 2010). Inclusion of albedo neutrons and the pion-electromagnetic (π/EM) cascade induced in the atmosphere have a large impact on the shielding calculation, especially on Mars surface. In fact, recent calculations with the modified HZETRN code (Slaba et al., 2013) suggest that aluminum shielding would always increase the equivalent dose on the Mars surface, while in deep space a reduction in dose is observed only below ~40 g/cm^2. On the other hand, HZETRN-π/EM transport code predicts that both dose equivalent and effective dose decrease monotonically with increasing polyethylene thickness in deep space and on Mars (Slaba et al., 2013).

4. Accelerator tests

Shielding transport calculations can use deterministic codes, such as the HZETRN used by NASA (Wilson et al., 1991), or Monte Carlo codes, such as GEANT4 (Matthiä et al., 2008), used by ESA, PHITS (Sato et al., 2011) and FLUKA (Trovati et al., 2006). Transport codes heavily rely on measured nuclear cross-sections. Even cross-sections for protons, which have been studied extensively, both experimentally and theoretically, show disagreements by a factor of 2 between the values calculated from models and measurements. To reduce the uncertainties in any radiation transport code being used for such calculations, precise measurements of interaction cross-sections are required against which to benchmark the codes. An extensive database of current measured cross-sections has been recently compiled by NASA (Norbury and Miller, 2012), and this work is very useful to highlight the missing values.

For composite materials, new shields based on nanomaterials, proprietary screens with undisclosed exact composition, complex in situ planetary resources, and so forth, code predictions have high uncertainties or may be completely lacking. Accelerator-based

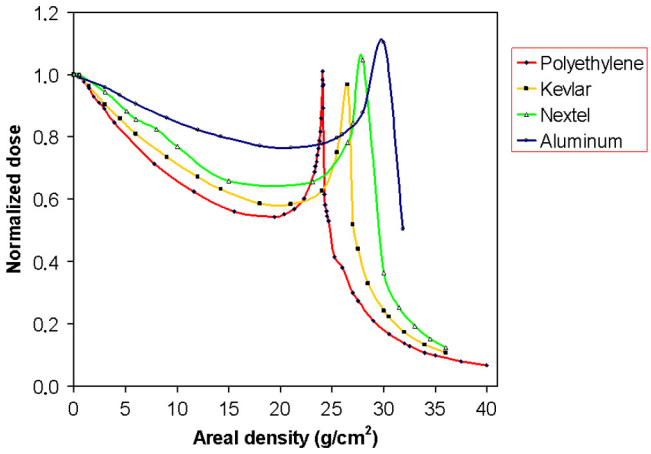

Fig. 4. Measured Bragg curve of 1 GeV/n Fe ions in polyethylene, aluminum, Kevlar, and nextel. The normalized dose is plotted vs. the thickness in g/cm^2. Materials effective for GCR shielding have a higher initial slope δD and shorter range. Polyethylene is clearly better than Al, and Kevlar is close to polyethylene. Measurements at the Brookhaven National Laboratory (Upton, NY), figure modified from Lobascio et al. (2008).

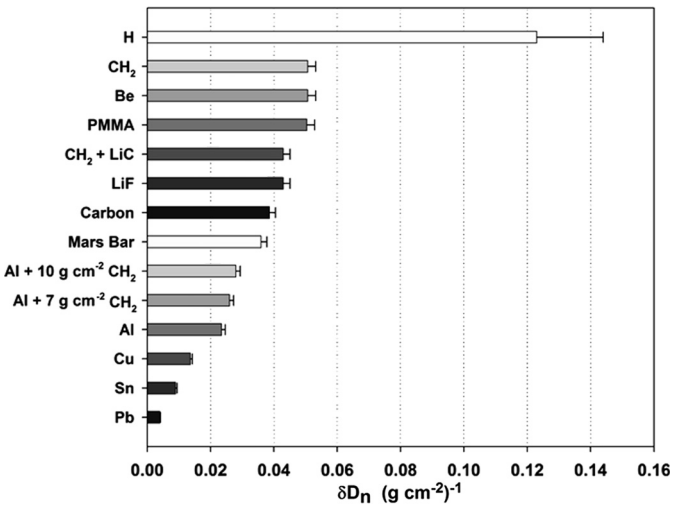

Fig. 5. Dose attenuation properties of a variety of shielding materials exposed to 1 GeV/n ^{56}Fe-ions. Bragg curves were measured by the LBL group at the Brookhaven National Laboratory. δD represents the initial slope of the Bragg curve (Eq. (5)), extrapolated to zero-thickness. Plot modified from Zeitlin et al. (2006), courtesy of Cary Zeitlin.

measurements are in those cases an essential tool to characterize the shield. The simplest test is the measure of the Bragg curve using heavy ions at high energy (Fig. 4). Under these conditions, the dose-depth curve presents a clear decrease before the Bragg peak, and the initial slope of the curve is approximately linear with the mass thickness. To describe this behavior, we can note that the fluence $F(x)$ of the incident ions at a distance x in the shield can be written as:

$$F(x) = F_0 e^{-\frac{\sigma N_A \rho x}{A_T}} \tag{4}$$

For small thickness x, the stopping power S is constant, and if we assume that the entire dose is deposited by the incident projectile, we have:

$$\delta D = \frac{D(x) - D_0}{D_0} \approx -\frac{\sigma N_A}{A_T}\rho x \tag{5}$$

The percentage dose reduction is linear with the areal density, and the slope is the fragmentation cross-section per unit target mass (described in Eq. (3)). Hence, the percentage dose reduction per unit mass thickness extrapolated to zero target thickness provides a simple measure of the shielding effectiveness per unit mass (Zeitlin et al., 2006).

Eq. (5) is obviously a crude approximation, not only because S is assumed to be constant, but especially because the dose is also deposited by the projectile fragments. The production cross section can be approximated as:

$$\sigma(Z_0 \to Z_f) \approx \frac{A_T}{N_A \rho x}\frac{N_f}{N_0} \tag{6}$$

where N_f represents the number of nuclei f produced by the fragmentation of N_0 projectiles in a mass thickness ρx. The ratio D_f/D_0 of the doses deposited by the N_f fragments and the N_0 projectiles is the ratio of the stopping powers, which is approximately proportional (Eq. (1)) to the ratio z_f^2/z_0^2 of the atomic numbers of the fragment and the projectile. Neglecting multiple fragmentations, it can be easily shown that:

$$\frac{D(x)}{D_0} \approx e^{-\frac{\sigma N_A \rho x}{A_T}}\left(1 + \frac{N_A \rho x}{A_T z_0^2}\sum_{i=1}^{n}\sigma_i z_i^2\right) \tag{7}$$

where σ is the total fragmentation cross-section of the projectile (Eq. (2)), $z_0 = n+1$ the atomic number of the projectile, and σ_i the production cross-section of the fragment of charge $z_i < z_0$ (Eq. (6)).

A large database of measurements of percentage dose reduction per unit thickness was collected by the Lawrence Berkeley Laboratory (LBL) group in a set of experiments at the Brookhaven National Laboratory in Upton, NY (Fig. 5) (Zeitlin et al., 2005). The same method has been used to estimate the shielding effectiveness of Kevlar and Nextel (Fig. 4) (Lobascio et al., 2008), commonly used against micrometeorites in space structures, and of the composite materials in the walls of the Columbus module on the ISS (Silvestri et al., 2011). ESA is currently sponsoring a set of measurements at GSI in Germany to test in situ planetary materials (Mars and moon regolith) and new materials with very high hydrogen content and excellent structural properties (Fig. 6).

Interestingly, the LBL group compared the measured percentage dose reduction per unit thickness, using a single heavy ion at a single energy, with a Monte Carlo simulation of the total GCR traversing the same shielding, therefore simulating the real attenuation expected in space (Guetersloh et al., 2006). The results are shown in Fig. 7. The measured data are higher than the estimates for the total GCR, because of the high contribution of protons, which of course do not fragment, to the total dose in space. On the other hand, measured attenuation for 1 GeV/n ions is slightly lower than the estimates for the heavy ion component in the GCR. This is probably caused by the contribution of higher energy ions in space (Guetersloh et al., 2006). Therefore, whilst 1 GeV/n Fe-ions give a reasonable proxy of the heavy ion component of the GCR for small thickness, a better quantitative agreement is expected for measurements at higher energies.

Accelerator tests of shielding materials can also provide other important data for the characterization of the shielding materials, such as microdosimetric spectra and neutron yields and energy spectra at different angles. Material tests at high-energy accelerators are therefore an important research tool for the assessment of the shielding effectiveness of novel materials.

5. Active shielding

Active shielding involves the generation of electromagnetic fields to deflect space radiation. Several approaches have been proposed (Spillantini et al., 2007):

- Electrostatic shield
- Plasma shield

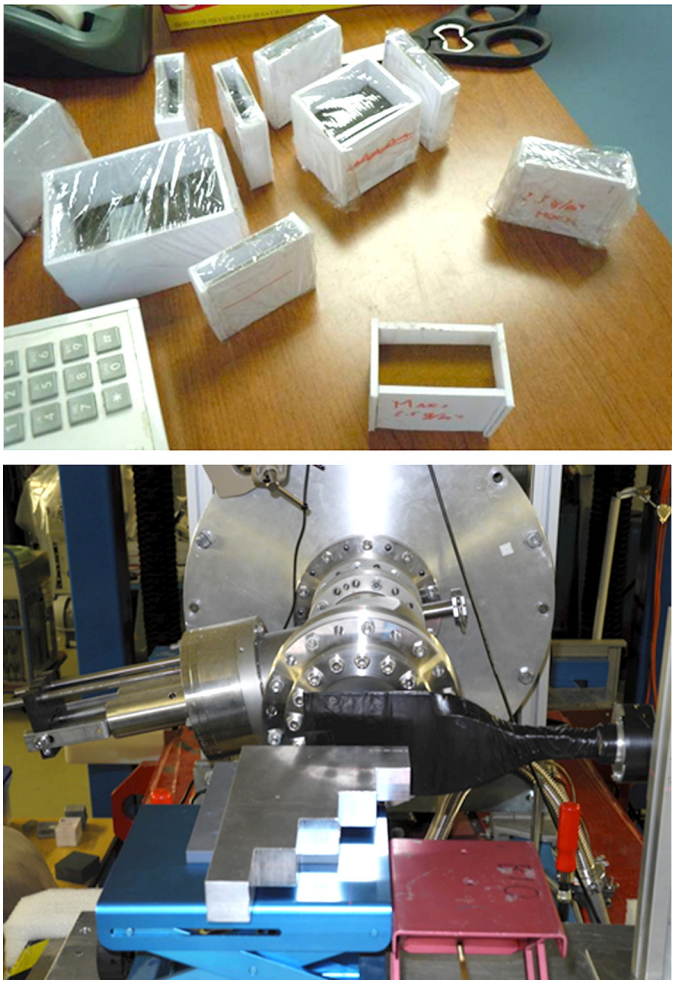

Fig. 6. Mars (yellow) and moon (brown) regolith targets (top pictures) irradiated at GSI for measurements of dose attenuation. In the bottom photograph, a plastic scintillator is shown to monitor the beam in the Cave A of the SIS18 accelerator at GSI. A stair target in Al is also shown. This target shape is useful for measurements of the Bragg curve. (For interpretation of the references to color in this figure legend, the reader is referred to the web version of this article.)

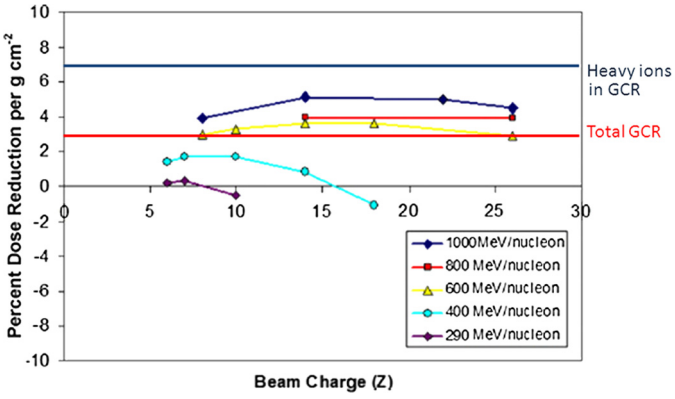

Fig. 7. Measured dose attenuation of heavy ions with different charge and velocity in 2.83 g/cm^2 polyethylene. Measurements were performed by the LBL group as described in Zeitlin et al. (2006). The data are compared with simulations of the dose attenuation of the whole GCR (red line) or of the heavy ion ($Z \geqslant 3$) component in the GCR (blue line) below the same polyethylene thickness. The GCR flux was calculated with the Badhwar–O'Neill model, assuming a solar deceleration parameter close to the solar maximum. Transport of the GCR through polyethylene was simulated by the BBFRAG simulation code. Figure modified from Guetersloh et al. (2006), courtesy of Cary Zeitlin. (For interpretation of the references to color in this figure legend, the reader is referred to the web version of this article.)

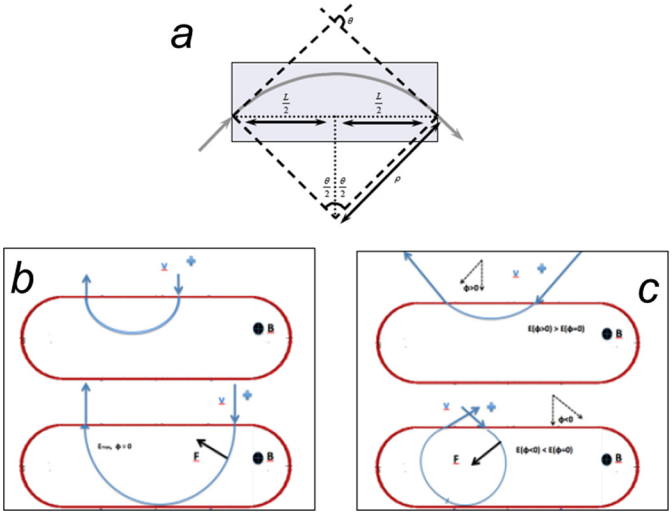

Fig. 8. Principles of magnetic shielding. a) Deflection by an angle θ of charged particles in a uniform dipolar magnetic field; b) magnetic field repulsion for particle traveling in a radial direction, orthogonal to a toroidal axis; c) magnetic field repulsion for particle traveling in a radial direction, at an angle φ with respect to the toroidal axis. Graphics from Battiston et al. (2011), courtesy of Roberto Battiston.

- Confined magnetic field
- Unconfined magnetic fields

For magnetic shielding, we can consider a uniform dipolar field B which deflects the impinging charged particles by an angle θ. From Fig. 8a, we can see that $\sin(\theta/2) = L/2\rho$ and for small angles:

$$\theta \approx 2 \cdot \frac{L}{2\rho} = \frac{BL}{B\rho} = \frac{BL}{R} \tag{8}$$

where $R = B\rho = pc/Ze$ is the particle rigidity. In principle, the value of BL may be chosen to protect efficiently any geometric volume up to the rigidity cutoff, where the residual radiation dose represented by the penetrating particles is either zero or acceptable by the radiation protection standards. However, this implies very large magnetic fields to protect a volume corresponding to the spacecraft, considering that $R[\mathrm{Tm}] = 3.3356\ p[\mathrm{GeV}/c]$. For instance, 1 GeV/n ions of the CNO group and up to iron have magnetic rigidity over 11 Tm, while 10 GeV protons exceed 35 Tm. These high magnetic fields can only be achieved using superconducting magnets.

Most of the recent efforts concentrate on confined magnetic fields. In particular, toroidal field configurations have been studied in the literature and quantitative estimates of the expected dose rates for a typical mission to Mars have been calculated (Hoffman et al., 2004; Choutko et al., 2004; Spillantini, 2010). Toroidal fields have the advantage of confining the field outside the habitable module, avoiding long exposure of the astronauts to an intense, static magnetic field, and, at the same time, have a null net dipole moment, which avoids torques induced by the Earth or by the interplanetary magnetic field. The principle of the toroidal shield is shown in Fig. 8 (Battiston et al., 2011). Particles entering the magnetic volume defined by the coils (red), will experience the Lorenz force $F = qvB\sin\varphi$. At $\varphi = 0$ (Fig. 8b), the maximum gyroradius r for protection is the total coil thickness L. It is given by the formula:

$$r = \frac{p_\perp}{qB} = \frac{m\gamma v}{kB} \tag{9}$$

where $k = 0.3$ GeV/Tm. For $\varphi \neq 0$ (Fig. 8c), particles can penetrate the shield for $r \geqslant L/2$. The corresponding kinetic energy (Eq. (9)) is

Table 3
Comparison of the confined field configurations: 1 – double-toroid-solenoid (Hoffman et al., 2004), 2 – endcap-toroid-barrel-toroid (Choutko et al., 2004) and 3 – barrel toroid (Spillantini, 2010).

Configuration	Hoffman et al. (2004)	Choutko et al. (2004)	Spillantini (2010)
Magnet mass (t)	300–1600[(1)]	31[(2)]	10–20[(3)]
BL (Tm)	15.6	17	20
Flux reduction factor	10	4–7	5
Diameter/length[(4)] (m)	10/10	9.6/8.5	8/10
Shielded volume (m^3)	116	69	63

(1) Total mass including coils, mechanical structure, cyrocooler, liquid helium.
(2) Quoted as "magnet system weight".
(3) Cold mass (superconducting cable and stabilizing material) × 1.5.
(4) Dimensions of cylindrical envelope containing the magnet configuration.

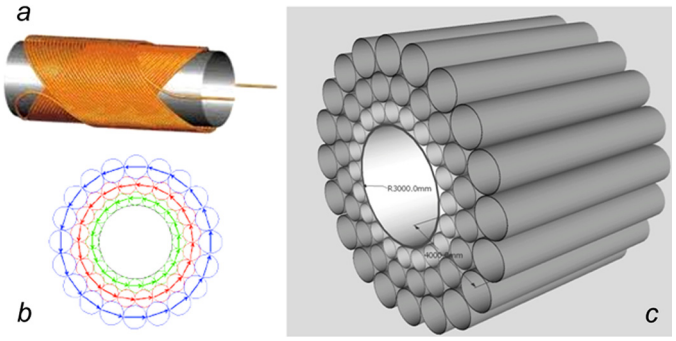

Fig. 9. The multiple double-helix coil solution is a new toroidal configurations under study in the SR2S project (Stokes et al., 2013). The double-helix coils shape (a) is designed so to create a very uniform dipole field within the volume of the cylinder, optimizing the effect of forces on the supporting structure. Multicoil structure (b) consisting of oriented double helix dipole coils produce a multi-toroidal field. A 3D image of this structure is given in the image (c). Images by SR2S Collaboration, courtesy of Roberto Battiston.

the cutoff radial energy. For example, $BL = 5$ Tm would correspond to a cutoff energy of 250 MeV for GCR protons.

Design studies with toroidal fields (Hoffman et al., 2004; Choutko et al., 2004; Spillantini, 2010) predict large shielding for GCR, ranging from 5 to 10, demonstrating the effectiveness of active toroidal magnetic systems (Table 3). The estimates of the magnetic shielding system weight vary substantially among the studies. However, since these weight estimates are 1–2 orders of magnitude lower than passive shields exhibiting similar shielding properties, these studies are a good starting point for further developments in this field.

The experience gained during the development of the Alpha Magnetic Spectrometer (AMS) (Battiston, 2008) superconducting magnet has been very useful to develop ideas and techniques to be applied to radiation shield for exploration missions. In this framework, conceptual designs of a magnetic configuration optimized for a Mars mission have been proposed by the AMS group within the SR2S project, started in January 2013 with EU support (Stokes et al., 2013). The SR2S concept is based on a modular multi-toroid concept. Each toroid is composed by several superconducting coils. The coil shape (race-track, D-shape or double-helix) will be chosen in order to optimize the magnet performance and the mechanical structure and to save weight. Intermediate temperature superconducting cables can improve the current/field performances of MgB_2 cables, to exploit their low weight, high current potential while operating above liquid Helium temperature (10–15 K) to exploit simplified gaseous He cooling. Recirculation of the cooling fluid (gas) through a cooling circuit can ensure long term operation in space. Examples of multi-toroidal configurations using the double-helix coil are given in Fig. 9.

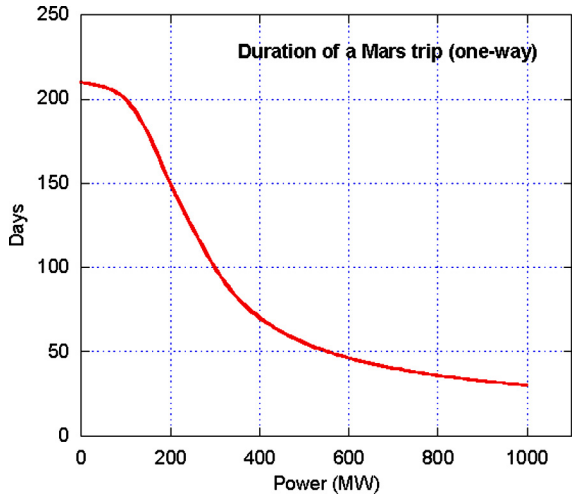

Fig. 10. Predicted duration of a Mars trip (one-way) as a function of the NEP thruster power at constant $I_{sp} = 320\,780$ m/s. The duration at $P = 0$ correspond to conventional chemical propulsion. For an electric thruster, the conversion efficiency is about 1/3 and therefore 1 MW NEP requires 3 MW thermal power. Figure adapted from Durante and Bruno (2010), courtesy of Claudio Bruno.

The design of a magnetic system for radiation shielding implies enormous technical difficulties. The toroidal field must surround a cabin large enough to host the astronauts for a long trip. Such a huge magnetic system cannot be launched as a whole, so it has to be assembled in orbit. Moreover, the system should be redundant: the failure of the magnet cannot leave the crew without protection. Progress in this field can eventually lead to a breakthrough in space radiation shielding, but practical solutions are not expected in the near future. Generally speaking, active shielding will always be combined to passive shielding, and the combination of the two strategies may be beneficial. A recent computational model using HZETRN suggests that, in a combined screen, passive shielding has greater impact for low magnetic bending power and in the end-cap regions (Washburn and et al., 2014). Bending powers greater than 15 Tm and passive shielding thicknesses greater than 40 g/cm^2 have a limited impact on further reducing dose equivalent values (Slaba et al., 2013; Washburn and et al., 2014).

6. Propulsion

The most effective countermeasure for the radiation risk would certainly be reducing the transit time (Durante and Bruno, 2010). As shown in Table 1, most of the dose is accumulated in deep space during the travel to/from Mars, and the daily dose on Mars (measured by MSL, Hassler et al., 2014) can further be reduced by thick in situ shielding. Moreover, a reduced transit time would minimize all the other health problems associated to prolonged microgravity and isolation.

However, use of innovative propulsion systems is still at an experimental phase. An interplanetary propulsion system featuring simultaneously high thrust (F) and high specific impulse (I_{sp}) is necessary. Impulse and thrust are connected by the formula:

$$I_{sp} = \frac{F}{\dot{m}} \tag{10}$$

where $\dot{m}$ is the mass consumption rate. The larger the I_{sp}, the less propellant is consumed to produce a given thrust. In view of the presumable initial mass of the interplanetary vehicle (≈100–300 metric tons), thrust ~10^3 kN would be required to impart sufficiently large trans-orbital momentum. Since jet power scales with $(I_{sp})^3$, thrust of the order 10^3 kN and I_{sp} around

1000 seconds imply power in the 10^6 kW range (Czysz and Bruno, 2009). Reducing the transit time to about one month using GW electric power engines (Fig. 10) would push the radiation dose for a Mars mission below 100 mSv (Durante and Bruno, 2010). This power cannot be achieved by chemical propulsion, and will require nuclear thrusters: nuclear thermal rockets (NTR) or nuclear electric propulsion (NEP). Although a NTR may reach high enough power, their massive propellant requirement is a substantial shortcoming. A hybrid NTP/NEP system seems to be necessary (Bruno et al., 2013). This hybrid system is called nuclear thermal-electric rocket (NTER) (Dujarric et al., 2013). The components of the exploration vehicle, including the NTER propulsion module and its propellant tanks, should be launched separately to LEO and assembled in orbit. The crew should be launched in a capsule, such as Orion, using a conventional launcher, directly to the rendezvous point. NTER is turned on in high thrust mode for around one hour in order to place impulsively the exploration vehicle on a fast transfer trajectory to Mars. It should be noted that the NTER concept poses further issues of shielding for the crew, which would need to be protected from radiation following the reactor shut-down.

7. Conclusions

Radiation risk is a major hindrance to human exploration of Mars. Current risk estimates support the view that the mission will not be possible without appropriate countermeasures. Biological countermeasures are not yet mature, and much research is concentrating on this topic (Kennedy, 2014). Among physical countermeasures, passive shielding is the only one presently available, but it is unlikely to be able to reduce the dose to an acceptable level, within the weight constraints of the launchers. Novel shielding materials can however give a significant reduction, and they can be tested in dedicated accelerator experiments. Active shielding, especially toroidal magnetic configurations are very promising, but still not mature enough for spaceflight. The best solution to the space radiation problem, as well as of the other health risks related to microgravity and isolation, is reduction of the transit time. This can only be achieved using nuclear propulsion, possibly a mixed system combining thermal and electric nuclear power (NTER), but this field also needs major developments for practical applications.

Planners of the first mission to Mars will probably look for combinations of different approaches: passive shielding (including a storm shelter against SPE) and transit time, with the latter incorporating decisions about trajectory (such as the one selected in the Inspiration Mars plan) and timing (e.g. at solar minimum to reduce the chance of SPE, or solar maximum to reduce chronic GCR exposure). Active shielding and NTER are probably the future options for later exploration missions, such as to the asteroid belt and the outer planets and their moons.

References

Battiston, R., 2008. The antimatter spectrometer (AMS-02): A particle physics detector in space. Nucl. Instrum. Methods Phys. Res., Sect. A, Accel. Spectrom. Detect. Assoc. Equip. 588, 227–234.

Battiston, R., et al., 2011. Active radiation shield for space exploration missions. Final Report ESTEC Contract N° 4200023087/10/NL/AF (ARSSEM). ESA, Nordwijk, The Netherlands.

Bruno, C., Durante, M., Dujarric, C., 2013. Propulsion requirements for a safe human exploration of Mars. IAC-13-C4.7.8. Beijing, China.

Choutko, V., Hofer, H., Ting, S.C.C., 2004. The AMS experiment and magnet Faraday cage for human space exploration. In: NASA Active Radiation Shielding Workshop. Ann Arbor, MI.

Cucinotta, F.A., et al., 2013. How safe is safe enough? Radiation risk for a human mission to Mars. PLoS ONE 8, e74988.

Czysz, P.A., Bruno, C., 2009. Future Spacecraft Propulsion Systems. Springer-Praxis, London. Chapter 7.

Drake, B.G., Hoffman, S.J., Beatty, D.W., 2010. Human exploration of Mars, Design Reference Architecture 5.0. In: Aerospace Conference. IEEE, pp. 1–24.

Dujarric, C., Santovincenzo, A., Summerer, L., 2013. The Nuclear Thermal Electric Rocket: a proposed innovative propulsion concept for manned interplanetary missions. In: Progress in Propulsion Physics. In: EUCASS Book Series, vol. 4. Torus Press, Moscow, pp. 293–312.

Durante, M., Bruno, C., 2010. Impact of rocket propulsion technology on the radiation risk in missions to Mars. Eur. Phys. J. D 60, 215–218.

Durante, M., Cucinotta, F.A., 2008. Heavy ion carcinogenesis and human space exploration. Nat. Rev. Cancer 8, 465–472.

Durante, M., Cucinotta, F.A., 2011. Physical basis of radiation protection in space travel. Rev. Mod. Phys. 83, 1245–1281.

Durante, M., Kronenberg, A., 2005. Ground-based research with heavy ions for space radiation protection. Adv. Space Res. 35, 180–184.

Guetersloh, S., et al., 2006. Polyethylene as a radiation shielding standard in simulated cosmic-ray environments. Nucl. Instrum. Methods Phys. Res., Sect. B, Beam Interact. Mater. Atoms 252, 319–332.

Hassler, D.M., et al., 2014. Mars' surface radiation environment measured with the Mars Science Laboratory's Curiosity Rover. Science 343, 1245267.

Hoffman, J., Fisher, P., Batishchev, O., 2004. Use of superconducting magnet technology for astronauts radiation protection. NASA Institute for Advanced Concepts, Phase 1 Report Final. Bull. Am. Phys. Soc. 49, 261.

ISECG, 2013. Global Exploration Roadmap. NASA NP-2013-06-945-HQ, http://www.globalspaceexploration.org/.

Kennedy, A., 2014. Biological effects of space radiation and developments of effective countermeasures. Life Sci. Space Res. 1, 10–43. In this issue.

Kodaira, S., et al., 2014. Verification of shielding effect by the water-filled materials for space radiation in the International Space Station using passive dosimeters. Adv. Space Res. 53, 1–7.

Lobascio, C., et al., 2008. Accelerator-based tests of radiation shielding properties of materials used in human space infrastructures. Health Phys. 94, 242–247.

Matthiä, D., Sihver, L., Meier, M., 2008. Monte Carlo calculations of particle fluences and neutron effective dose rates in the atmosphere. Radiat. Prot. Dosim. 131, 222–228.

NASA, 2005. Bioastronautics Roadmap. NASA/SP-2004-6113. http://humanresearchroadmap.nasa.gov/.

NASA, 2007. Space flight human system standard volume I; Crew health. NASA STD-3001.

National Research Council, 2006. Health Risks from Exposure to Low Levels Ionizing Radiation: BEIRVII. National Academy Press.

Norbury, J.W., Miller, J., 2012. Review of nuclear physics experimental data for space radiation. Health Phys. 103, 640–642.

Ozasa, K., et al., 2012. Studies of the mortality of atomic bomb survivors, Report 14, 1950–2003: an overview of cancer and noncancer diseases. Radiat. Res. 177, 229–243.

Sato, T., et al., 2011. Evaluation of dose rate reduction in a spacecraft compartment due to additional water shield. Cosm. Res. 49, 319–324.

Shavers, M.R., et al., 2004. Implementation of ALARA radiation protection on the ISS through polyethylene shielding augmentation of the Service Module Crew Quarters. Adv. Space Res. 34, 1333–1337.

Siegel, R., Naishadham, D., Jemal, A., 2013. Cancer statistics. CA Cancer J. Clin. 63, 11–30.

Silvestri, M., et al., 2011. Impact of spacecraft-shell composition on 1 GeV/nucleon ^{56}Fe ion-fragmentation and dose reduction. IEEE Trans. Nucl. Sci. 58, 3126–3132.

Slaba, T.C., et al., 2010. Coupled neutron transport for HZETRN. Radiat. Meas. 45, 173–182.

Slaba, T.C., et al., 2013. Radiation shielding optimization on Mars. NASA/TP-2013-217983.

Spillantini, P., 2010. Active shielding for long duration interplanetary manned missions. Adv. Space Res. 43, 900–916.

Spillantini, P., et al., 2007. Shielding from cosmic radiation for interplanetary missions: active and passive methods. Radiat. Meas. 42, 14–23.

Stokes, B., et al., 2013. Space radiation superconductive shield. Doc N° SR2S-WPD51.2, EU FP7. http://sr2s.eu/.

Tito, D., et al., 2013. Feasibility analysis for a manned Mars free-return mission in 2018. In: Aerospace Conference. IEEE.

Trovati, S., et al., 2006. Human exposure to space radiation: role of primary and secondary particles. Radiat. Prot. Dosim. 122, 362–366.

Washburn, S.A., et al., 2014. Analytical-HZETRN model for rapid assessment of active magnetic radiation shielding. Adv. Space Res. 53, 8–17.

Wilson, J.W., et al., 1991. Transport methods and interactions for space radiations. NASA RP 1257.

Wilson, J.W., et al., 1997. Shielding strategies for human space exploration. NASA CP3370.

Zeitlin, C., et al., 2005. Shielding and fragmentation studies. Radiat. Prot. Dosim. 116, 23–24.

Zeitlin, C., et al., 2006. Measurements of materials shielding properties with 1 GeV/nuc ^{56}Fe. Nucl. Instrum. Methods Phys. Res., Sect. B, Beam Interact. Mater. Atoms 252, 308–318.

Zeitlin, C., et al., 2013. Measurements of energetic particle radiation in transit to Mars on the Mars Science Laboratory. Science 340, 1080–1084.